The antikick strikes back: Recoil velocities for nearly extremal binary black hole mergers in the test-mass limit

Alessandro Nagar,[1] Enno Harms,[2] Sebastiano Bernuzzi,[2] and Anıl Zenginoğlu[1]

[1]*Institut des Hautes Etudes Scientifiques, 91440 Bures sur Yvette, France*
[2]*Theoretical Physics Institute, University of Jena, 07743 Jena, Germany*

Gravitational waves emitted from a generic binary black hole merger carry away linear momentum anisotropically, resulting in a gravitational recoil, or "kick," of the center of mass. For certain merger configurations the time evolution of the magnitude of the kick velocity has a local maximum followed by a sudden drop. Perturbative studies of this "antikick" in a limited range of black hole spins have found that the antikick decreases for retrograde orbits as a function of negative spin. We analyze this problem using a recently developed code to evolve gravitational perturbations from a point particle in Kerr spacetime driven by an effective-one-body resummed radiation reaction force at linear order in the mass ratio $\nu \ll 1$. Extending previous studies to nearly extremal negative spins, thus complementing current numerical relativity knowledge about the recoil, we find that the well-known decrease of the antikick is overturned and, instead of approaching zero, the antikick increases again to reach $\Delta v/(c\nu^2) = 3.37 \times 10^{-3}$ for dimensionless spin $\hat{a} = -0.9999$. The corresponding final kick velocity is $v_{\text{end}}/(c\nu^2) = 0.076$. We interpret the antikick result analytically by means of the *quality factor Q* of the linear momentum flux, that is used to quantify the amount of nonadiabaticity of the emission process. We show that, besides capturing qualitatively the global properties over the whole spin range, Q actually predicts the return of the antikick for $\hat{a} \to -1$. Since Q is computed only from the, gauge-invariant, flux of linear momentum, the herein presented verification of its reliability advocates its systematic use also in numerical relativity calculations. In addition, we also connect, in a new way, the properties of the flux to the noncircular character of the plunge dynamics, highlighting the central role of subdominant waveform multipoles in shaping the characteristic interference pattern exhibited by the linear momentum flux as $\hat{a} \to -1$.

I. INTRODUCTION

The anisotropic emission of gravitational radiation in coalescing black hole binaries carries away linear momentum from the system, which results in a net recoil of the center of mass. This gravitational recoil, or "kick," can be related to a delicate and complicated interference between the gravitational wave (GW) multipoles [1]. In the test-mass limit the recoil can be computed using perturbative methods by modeling the small black hole as a point particle. Perturbative studies are crucial to study the basic features of the interference pattern among different multipoles. The detailed understanding of the physics of the recoil in the perturbative regime is important also for comparable mass binaries. As pointed out in Ref. [2], extrapolation from the test-mass results delivers quantitative agreement with numerical relativity data for nonrotating black holes. Furthermore, for a rotating central black hole only the perturbative framework can systematically probe the extremal regime.

Recoil computations in the test-mass limit were performed recently by two groups using time domain calculations. The case with a nonrotating central black hole was studied in [3] solving the Regge-Wheeler-Zerilli (RWZ) equations for gravitational metric perturbations. The case with a rotating

central black hole was studied in [4] (SKH hereafter) solving the Teukolsky equation for gravitational curvature perturbations. The SKH analysis was limited to spin magnitudes $|\hat{a}| \leq 0.9$, where $\hat{a}$ is the dimensionless angular momentum parameter. In particular, SKH studied the drop in the time evolution of the recoil velocity, or "antikick" [1,5], as a function of spin, and found that it is "essentially nonexistent" for large spin retrograde coalescences.

Building on recent progress in solving numerically the Teukolsky equation with a point-particle source in the time domain [6], we revisit the SKH analysis and extend it to *nearly extremal* spin values, particularly focusing on the retrograde case with spin parameters up to $\hat{a} = -0.9999$. The extension of the parameter space reveals a new phenomenon: the antikick significantly reappears for $-1 < \hat{a} < -0.9$, i.e., it returns to values comparable to those for moderately spinning configurations with $\hat{a} \sim -0.2$. We explain this phenomenon by analyzing and relating the dynamics of the plunge and the GW linear momentum flux. As noted long ago by Damour and Gopakumar [7] (DG hereafter) the time evolution of the recoil velocity (also for the comparable mass-ratio case) and, in particular, the existence of an antikick can be directly connected to the nonadiabatic emission of linear momentum during the plunge. Following DG, the behavior

of the antikick as a function of $\hat{a}$ is understood analytically and quantified in a "quality factor" Q associated to the maximum of the GW linear momentum flux (Sec. IV). This understanding of the antikick relies on gauge-invariant notions and our systematic investigation of its efficiency advocates it as a useful alternative to previous discussions that emphasize the trajectory [8,9] or curvature distributions on the horizon [10].

To set the stage for our analysis, we discuss the dynamics of the system providing a quantitative measure for its nonadiabaticity (Sec. II), and point out interesting properties of the GW linear momentum flux (Sec. III): as $\hat{a} \to -1$, the linear momentum flux shows a characteristic, multi-peaked interference pattern that can be explained by the increased importance of the subdominant waveform multipoles $0 \leq m < \ell$ during the plunge [6]. The behavior of the maximal and final recoil velocity is discussed and analytically explained in Sec. IV. We examine the accuracy of our results in the Appendix, including extremal positive spins, $+0.9 \leq \hat{a} \leq +0.9999$, that require special care.

We use geometric units $c = G = 1$. The dynamics of the particle is obtained using a Hamiltonian formulation [6,11] and expressed in dimensionless canonical variables.

II. DYNAMICS: MEASURING NONADIABATICITY

In the test-mass limit we model the black hole binary system by a central spinning black hole of mass M and a nonspinning particle of mass μ, such that $\nu = \mu/M \ll 1$. Our test-mass calculations follow the method developed in [3,12], extended to the Kerr background in [6]. The gravitational waveforms used to compute the flux of linear momentum are extracted at future null infinity with a perturbative method based on the solution of the Teukolsky equation in the time domain. The black hole spin is either aligned or antialigned with the orbital angular momentum. The relative dynamics is driven by an effective-one-body resummed analytic radiation reaction [13,14] at linear order in ν. For simplicity, we do not include horizon absorption [15,16], so that the radiation reaction only incorporates the angular momentum flux emitted to infinity, following [6]. Since our radiation reaction is certainly inaccurate as $\hat{a} \to 1$ (because of both the absence of horizon absorption and the lack of higher-order spin-dependent terms in the resummed flux at infinity [6,17]) our results for large, positive spin may be partly affected by systematic uncertainties. For this reason, we discuss in the main text only the spin range $-0.9999 \leq \hat{a} \leq +0.9$, while the more challenging[1] regime $+0.9 < \hat{a} \leq +0.9999$ is discussed separately in the

Appendix. Our main new findings are in the regime $\hat{a} \to -1$, where the analytic radiation reaction is robust. We work with mass ratio $\nu = 10^{-3}$; the spin configurations we consider are listed in Table 4 of [6].

The relative dynamics is started from postcircular initial data [12,20] and driven from inspiral to plunge by the radiation reaction. The transition from quasicircular inspiral to plunge depends on the spin-orbit coupling between the orbital angular momentum and the black hole spin through the Hamiltonian. It can be slowly varying and adiabatic [spin aligned with the orbital angular momentum, the last stable orbit (LSO) moves towards the horizon] or quickly varying and nonadiabatic (spin antialigned with the orbital angular momentum, the LSO moves away from the horizon). The net GW emission of linear momentum and the final value of the recoil velocity can be connected to the nonadiabatic character of the plunge dynamics [7]. (A similar argument has also been discussed recently in Refs. [8,9].) In the following, we introduce a quantitative measure of this nonadiabaticity in the plunge phase.

Consider the time derivative of the radial momentum in a tortoise coordinate $-\dot{p}_{r_*}$ (changed sign for clarity; see Ref. [6] for the precise definition). As shown in Ref. [6] (see Fig. 15 there), $-p_{r_*}$ is a monotonic function of time: it grows during the plunge attaining a finite maximum at the horizon. Its time derivative has a bell shape as displayed in Fig. 1 for a few representative values of $\hat{a}$. For convenience of comparison, the plot is done versus $t - t_{\text{LR}}$, where t_{LR} is
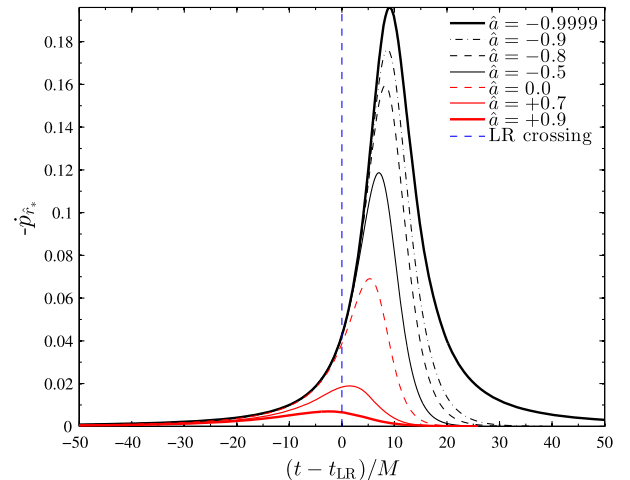

FIG. 1 (color online). Time evolution of $-\dot{p}_{r_*}$: the characteristic time scale of the curve $\tau^{\max}_{\dot{p}_{r_*}}$ [Eq. (1)] is a measure of the adiabaticity of the plunge. One finds that $\tau^{\max}_{\dot{p}_{r_*}}$ decreases from $\hat{a} = 0.9$ to $\hat{a} = -0.58$ (see also Table I), but then increases again. Such behavior is consistent with the analysis of the linear momentum flux [in particular with the increase of its "quality factor" Q, see Eq. (10) below] and the related peculiar time evolution of the recoil velocity as $\hat{a} \to -1$ (see Fig. 4). Note that $(t - t_{\text{LR}})/M = 0$ indicates the light-ring crossing time.

---

[1]Note that by "challenging" we refer here to the limits of the radiation reaction model and *not* to the solution of the Teukolsky equation using the methods of Refs. [6,18]. The inclusion of the higher-order post-Newtonian information of Ref. [19] in resummed form (not available at the moment) in the radiation reaction would certainly allow us to improve our approach.

the light-ring crossing time defined by $r_{\mathrm{LR}} \equiv r(t_{\mathrm{LR}})$ and $r_{\mathrm{LR}} = 2[1 + \cos(\frac{2}{3}\arccos(-\hat{a}))]$.

The spin-orbit interaction is repulsive for prograde orbits and attractive for retrograde orbits. Consistently, the distribution of $-\dot{p}_{r_*}$ is wider as $\hat{a} \to +1$ (slowly varying, adiabatic plunge dynamics) and narrower as $\hat{a} \to -1$ (quickly varying, nonadiabatic plunge dynamics). To quantify the spin dependence of the width of the curve, we define its characteristic variation time $\tau_{\dot{p}_{r_*}}^{\max}$ around its peak as

$$(\tau_{\dot{p}_{r_*}}^{\max})^2 = -\frac{\dot{p}_{r_*}}{\dddot{p}_{r_*}}\bigg|_{t=t_{\max}^{\dot{p}_{r_*}}}, \qquad (1)$$

where $t_{\max}^{\dot{p}_{r_*}}$ corresponds to the peak of $-\dot{p}_{r_*}$. The values of $\tau_{\max}^{\max}$ are listed in Table I. Note that $\tau_{\dot{p}_{r_*}}^{\max}$ *is not* monotonically decreasing when the spin decreases from positive to nearly extremal negative values (it is not possible to deduce this from Fig. 1, but see below Fig. 6). On the contrary, $\tau_{\dot{p}_{r_*}}^{\max}$ attains a global minimum for $\hat{a} \sim -0.58$. In order to obtain more accurate locations of minima with respect to the spins $\hat{a}$ we first identify the discrete minimum, then fit a parabola function through four points around it and finally assess the interpolated minimum as the minimum of this parabola. For values $\hat{a} \to -1$ $\tau_{\dot{p}_{r_*}}^{\max}$ grows again indicating that the dynamics becomes slightly more adiabatic again.[2] Such a simple quantitative characterization of the plunge is helpful in interpreting the following analysis of the linear momentum flux and the recoil velocity.

III. THE GW LINEAR MOMENTUM FLUX

Let us now analyze the GW linear momentum flux. We will see how the emission of linear momentum closely mirrors the plunge dynamics. Notably, the analysis of the flux (a gauge-invariant quantity) does not require having at hand a description of the dynamics and therefore can be directly applied to investigate also numerical relativity data.

In our simulations the GW linear momentum is emitted in the equatorial xy plane because we consider equatorial orbits (the black hole spin is either aligned or antialigned with the orbital angular momentum). Working with

RWZ-normalized variables $\Psi_{\ell m}^{(e)}$ the GW linear momentum flux reads[3]

$$\mathcal{F}^{\mathbf{P}} = \mathcal{F}_x^{\mathbf{P}} + i\mathcal{F}_y^{\mathbf{P}} = \sum_{\ell=2}^{\ell_{\max}} \mathcal{F}_\ell^{\mathbf{P}}$$

$$= -\frac{1}{8\pi}\sum_{\ell=2}^{\ell_{\max}}\sum_{m=-\ell}^{\ell}\bigg[ia_{\ell m}\dot{\Psi}_{\ell m}^{(0)}\dot{\Psi}_{\ell,m+1}^{(1)*}$$

$$+ b_{\ell m}\sum_{\epsilon=0,1}\dot{\Psi}_{\ell m}^{(\epsilon)}\dot{\Psi}_{\ell+1,m+1}^{(\epsilon)*}\bigg], \qquad (2)$$

where the real coefficients $(a_{\ell m}, b_{\ell m}) > 0$ are given by [3]

$$a_{\ell m} = 2(\ell-1)(\ell+2)\sqrt{(\ell-m)(\ell+m+1)}, \quad (3)$$

$$b_{\ell m} = \frac{(\ell+3)!}{(\ell+1)(\ell-2)!}\sqrt{\frac{(\ell+m+1)(\ell+m+2)}{(2\ell+1)(2\ell+3)}}, \quad (4)$$

ϵ is the parity of $(\ell+m)$, and the asterisk indicates complex conjugation.[4] For each value of ℓ, the contribution $\mathcal{F}_\ell^{\mathbf{P}}$ involves all ℓ and $\ell+1$ waveform multipoles [e.g., for $\ell = 2$ one deals with the $(\ell = 2, m = \{0, \pm 1, \pm 2\})$ and $(\ell = 3, m = \{0, \pm 1, \pm 2, \pm 3\})$, which amounts to seven independent multipoles because of $\Psi_{\ell m}^{*(\epsilon)} = (-1)^m \Psi_{\ell,-m}^{(\epsilon)}$]. Since we extracted gravitational wave multipoles up to $\ell_{\max} = 8$, we do not include $\ell = 9$ modes in $\mathcal{F}_8^{\mathbf{P}}$.

Figure 2 shows the modulus of the flux of linear momentum as a function of the retarded time u (see Ref. [6]) for $\hat{a} = -0.9999$ (top), $\hat{a} = -0.5$ (middle) and $\hat{a} = +0.9$ (bottom). Each labeled line on the plot corresponds to the sum $\sum_{\ell=2}^{\ell_{\max}} \mathcal{F}_\ell^{\mathbf{P}}$ in Eq. (2) up to the indicated $\ell_{\max}$. The vertical dashed line indicates the "merger time" u_{mrg} defined as the time of the peak of $|\Psi_{22}^{(0)}|$. To relate these figures with Fig. 1, as $\hat{a} \to -1$ one has $u_{\mathrm{mrg}} \approx t_{\mathrm{LR}}$, while as $\hat{a} \to 1$ one progressively gets $u_{\mathrm{mrg}} < t_{\mathrm{LR}}$. The precise quantitative information is collected in Table 4 of [6]: one has $t_{\mathrm{LR}} = 7321.7$ for $\hat{a} = -0.9999$, $t_{\mathrm{LR}} = 3321.3$ for $\hat{a} = -0.5$ and $t_{\mathrm{LR}} = 883.6$ for $\hat{a} = +0.9$ (the corresponding LSO crossing times are 6858.3, 2980.4 and 820.7).

Comparing the three plots in Fig. 2 one can directly extract that as $\hat{a} \to -1$: (i) the emission of linear momentum appears more localized in time (the three time axes show an equally sized range of $\sim 140M$), i.e., it becomes an

---

[2]Since p_{r_*} attains values larger than 1 around the light-ring crossing, as seen in Fig. 15 of Ref. [6], one may have some nonnegligible contribution of the radial part of the radiation reaction $\mathcal{F}_{r_*}$ as $\hat{a} \to -1$. This term is not included in the dynamics because of the current lack of a robust resummation strategy for the post-Newtonian expanded results of Ref. [21]. Still, we have verified that the inclusion of the leading-order term $\mathcal{F}_{r_*} = -\frac{5}{3}\frac{p_{r_*}}{p_\phi}\mathcal{F}_\phi$ (here p_ϕ is the mechanical angular momentum and $\mathcal{F}_\phi$ its resummed loss [6]) does not have any visible effect on the plunge dynamics. This makes us confident that indirect plunges are essentially geodesic.

[3]Note that our discussion on a rotating background could be formulated in terms of decompositions into azimuthal m modes only. But, despite the phenomenon of mode mixing [22,23], we stick to the full spin-weighted spherical harmonics decomposition, since in our setup the flux calculation in terms of m modes only is technically more involved due to the coupling between m and $m + 1$ in Eq. (2) (two different simulations).

[4]Note that Eq. (2) with the condition that ϵ is the parity of $\ell + m$ already implements the fact that the motion is planar, so that even-parity modes with $\ell + m =$ odd and odd-parity modes with $\ell + m =$ even are zero. In addition, Eq. (2) correctly exhibits the overall minus sign that was omitted by mistake in Ref. [3].
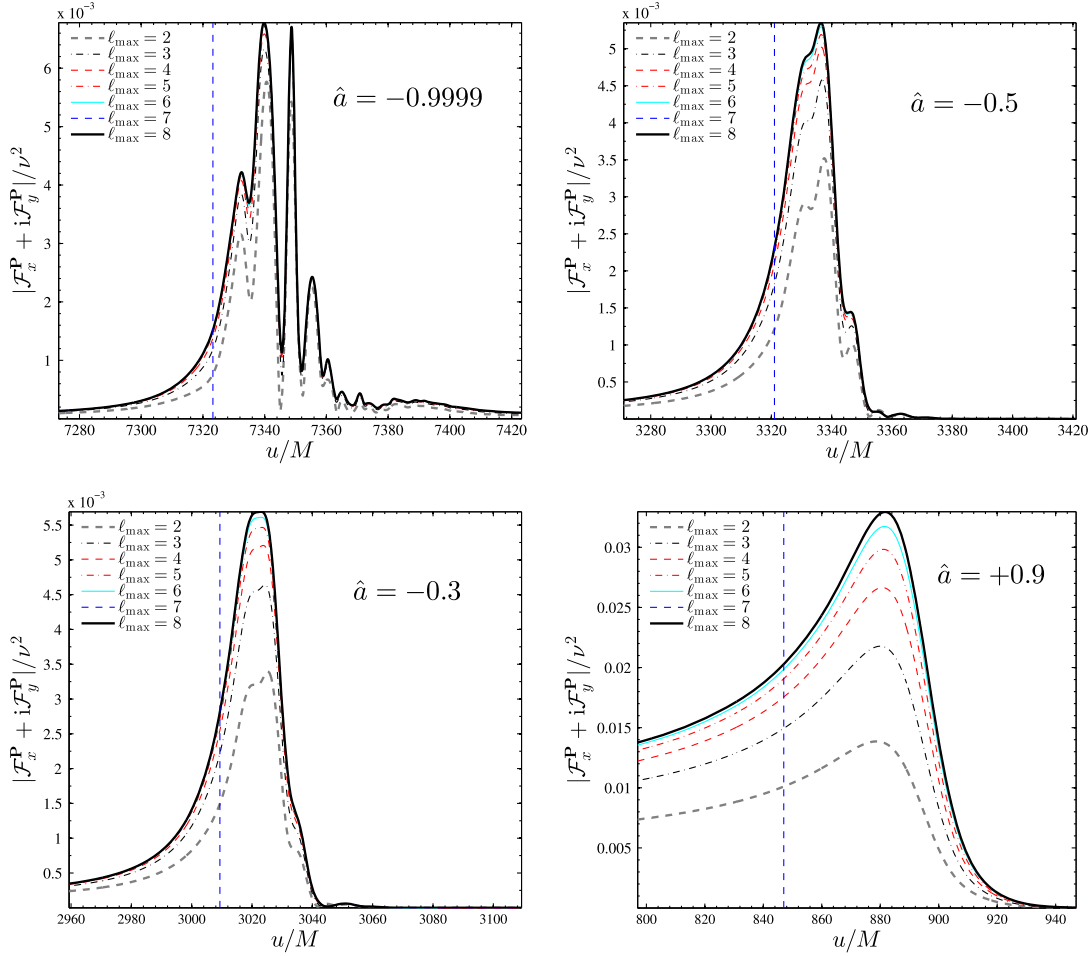
FIG. 2 (color online).   Modulus of the linear momentum flux for three representative values of $\hat{a}$. As $\hat{a} \to -1$, the emission of linear momentum occurs in a shorter time. The interference pattern seen for $\hat{a} = -0.9999$ is determined by the increased importance of the subdominant waveform multipoles with $0 \le m < \ell$ when $\hat{a} \to -1$ (see Ref. [6]) around merger u_{mrg} (defined as the peak of $|\Psi_{22}^{(0)}|$, dashed vertical lines). For $\hat{a} = -0.3$ the peak of the flux seems to actually be composed of two peaks of approximately the same height so close together that they purport to be one. Note that $u_{\mathrm{mrg}} \approx t_{\mathrm{LR}}$ as $\hat{a} \to -1$ and $u_{\mathrm{mrg}} < t_{\mathrm{LR}}$ as $\hat{a} \to 1$. See text for details.

impulsive phenomenon; (ii) the simple single-peak structure is replaced by a complicated interference pattern with several peaks of different amplitude and width.

This phenomenon mirrors strong destructive interference effects between the various terms entering Eq. (2). Such effect is maximal as $\hat{a} \to -1$ and progressively less apparent as $\hat{a}$ increases. It can be explained (see below) by the magnification of the subdominant $0 \le m < \ell$ modes during the late plunge and merger as $\hat{a} \to -1$. Since it is present already in the leading-order $\mathcal{F}_2^{\mathbf{P}}$ term (dashed line in the bottom panel of Fig. 2) it can be qualitatively understood by analyzing the behavior of this contribution only as a function of the black hole spin.

Setting $\ell_{\max} = 2$ the corresponding GW linear momentum flux $\mathcal{F}_2^{\mathbf{P}}$ can be seen as generated by the interference of the following seven terms:

$$\mathcal{F}_2^{\mathbf{P}} = \mathcal{F}_{223\text{-}3} + \mathcal{F}_{2\text{-}231} + \mathcal{F}_{2\text{-}221}$$
$$+ \mathcal{F}_{202\text{-}1} + \mathcal{F}_{203\text{-}1} + \mathcal{F}_{213\text{-}2} + \mathcal{F}_{2\text{-}130}. \quad (5)$$

The $\mathcal{F}_{lm\ell'm'}$ are obtained from Eq. (2) and explicitly read

$$\mathcal{F}_{223\text{-}3} = \frac{5}{\pi}\sqrt{\frac{6}{7}}\dot{\Psi}_{22}^{(0)}\dot{\Psi}_{3\text{-}3}^{(0)}, \quad (6a)$$

$$\mathcal{F}_{2\text{-}221} = \frac{2i}{\pi}\dot{\Psi}_{2\text{-}2}^{(0)}\dot{\Psi}_{21}^{(1)}, \quad (6b)$$

$$\mathcal{F}_{2\text{-}231} = \frac{1}{\pi}\sqrt{\frac{10}{7}}\dot{\Psi}_{2\text{-}2}^{(0)}\dot{\Psi}_{31}^{(0)}, \quad (6c)$$

$$\mathcal{F}_{202\text{-}1} = \frac{i}{\pi}\sqrt{6}\dot{\Psi}_{20}^{(0)}\dot{\Psi}_{2\text{-}1}^{(1)}, \quad (6d)$$

$$\mathcal{F}_{203\text{-}1} = \frac{2}{\pi}\sqrt{\frac{15}{7}}\dot{\Psi}_{20}^{(0)}\dot{\Psi}_{3\text{-}1}^{(0)}, \quad (6e)$$

$$\mathcal{F}_{213\text{-}2} = -\frac{1}{\pi}\frac{10}{\sqrt{7}}\dot{\Psi}_{21}^{(1)}\dot{\Psi}_{3\text{-}2}^{(1)}, \quad (6f)$$

$$\mathcal{F}_{2-130} = -\frac{1}{\pi}\sqrt{\frac{30}{7}}\dot{\Psi}_{2-1}^{(1)}\dot{\Psi}_{30}^{(1)}, \qquad (6g)$$

when using $\Psi_{\ell m}^{*(e)} = (-1)^m \Psi_{\ell,-m}^{(e)}$. References [6,17] pointed out that the breakdown of the circularity during the plunge as $\hat{a} \to -1$ (see Fig. 15 in Ref. [6]) makes each multipolar waveform amplitude higher and sharper around its own peak (which occurs near merger). In particular, for $0 \le m < \ell$ the peak amplitudes get amplified to values comparable to that of the leading $\ell = m = 2$ mode (the effect is particularly striking for the $m = 0$ modes). This phenomenon occurs on the short time scale of the plunge and thus also yields a magnification of the $\dot{\Psi}_{\ell m}^{(e)}$'s. One can then understand how the spin dependence of the various $\mathcal{F}_{lm\ell'm'}$ terms in Eqs. (6) can prompt complicated interference patterns via Eq. (5). To illustrate how this works in practice, Fig. 3 compares the real part of the seven partial contributions given by Eq. (6) for spins $\hat{a} \in \{-0.9999, -0.5, +0.9\}$. For $\hat{a} = -0.9999$ all terms in Eq. (6) are comparable. One sees that $\mathcal{F}_{202-1}$ and $\mathcal{F}_{2-231}$ are approximately in phase among themselves and in phase opposition to $\mathcal{F}_{213-2}$ and $\mathcal{F}_{223-3}$. When taking the modulus of the sum of all these contributions one understands the origin of the minima in the modulus of Fig. 2. Notably, the times of the minima in Fig. 2 correspond to the minima of $\mathcal{F}_{202-1}$ and $\mathcal{F}_{2-231}$, indicating that the interference pattern of the linear momentum flux reflects the enhancement of $(\Psi_{20}^{(0)}, \Psi_{21}^{(1)}, \Psi_{31}^{(0)})$. This is due to next-to-quasi-circular effects (driven by p_{r_*}) on the waveform, which become progressively more important during the plunge when $\hat{a} \to -1$.

By contrast, when $\hat{a} = +0.9$, $\mathcal{F}_{223-3}$ is much larger than the other terms, e.g., $\mathcal{F}_{2-231}$ and $\mathcal{F}_{202-1}$ do not contribute significantly. The negligible value of $\dot{\Psi}_{31}^{(0)}$ with respect to $\dot{\Psi}_{2-2}^{(0)}$ essentially removes the complicated behavior that one finds in $\mathcal{F}_{2-231}$ as $\hat{a} \to -1$, and this contribution is just dominated by the $\dot{\Psi}_{2-2}^{(0)}$ mode. Note in the bottom panel of Fig. 3 how the red and black lines are dephased by $\pi/2$, consistent with the dephasing due to complex conjugation.

Finally, focusing on the case $\hat{a} = -0.9999$ for definiteness, we note that the emission of linear momentum predominantly occurs in the time interval (7320,7360) around the largest peak of $|\mathcal{F}^{\mathbf{P}}|$; the interval is approximately the same where $-\dot{p}_{r_*}$ is significantly different from zero ($-\dot{p}_{r_*}$ peaks at $t_{\max}^{p_{r_*}} \approx 7331$). This supports the understanding that there is a strong correlation between the time variation of p_{r_*} and (the time derivatives of) the gravitational waveform around the light-ring crossing so to generate the narrow burst of linear momentum. For this value of the spin, we also note that the rather shallow peak of the modulus of the flux around $u/M \sim 7390$ is essentially driven by the quasi-normal-mode excitation. For $\hat{a} = -0.9999$ the modes are long-lasting, which explains why this peak is so shallow (see also the top panel of Fig. 3). The same feature, with the same explanation, is seen also for

$\hat{a} = -0.5$, though it is absent for $\hat{a} = +0.9$ (because quasinormal modes (QNMs) are damped much faster). We postpone to future work a detailed analysis of the QNM-driven features of the linear momentum flux.
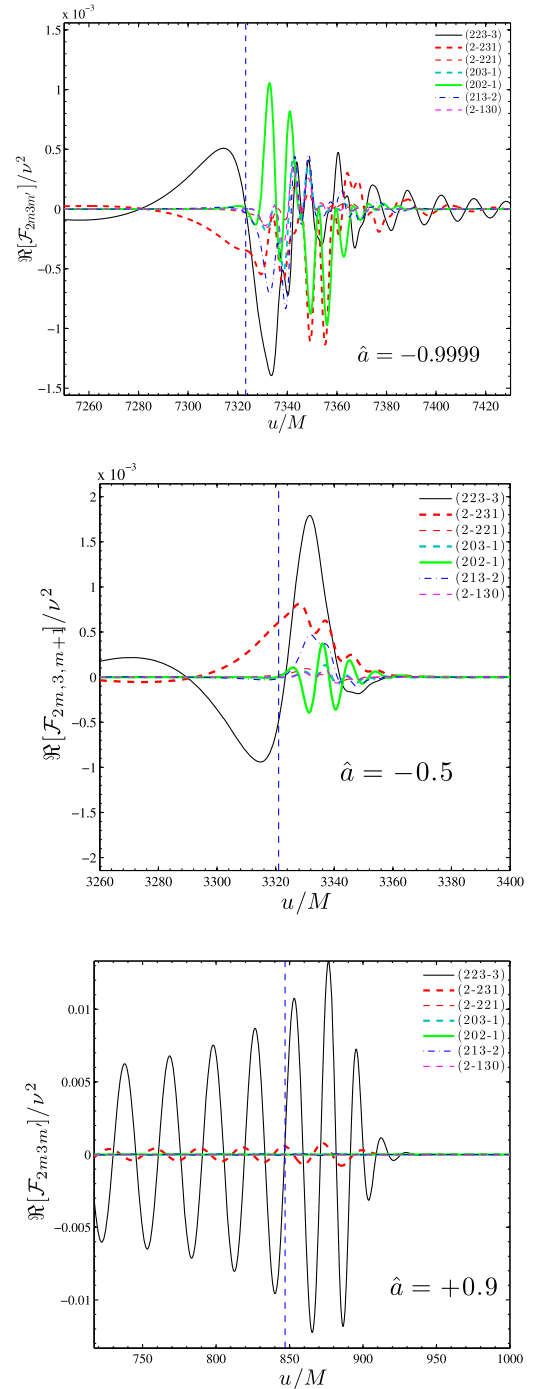

FIG. 3 (color online). Comparing the real part of the various terms entering the leading contribution $\mathcal{F}_2^{\mathbf{P}}$ to the linear momentum flux, Eq. (5). One sees that for $\hat{a} = -0.9999$ all terms in Eqs. (6a)–(6g) have comparable magnitudes around merger (defined as the peak of $|\Psi_{22}^{(0)}|$, dashed vertical lines). This prompts the interference pattern seen in the corresponding modulus in Fig. 2. Note that $u_{\mathrm{mrg}} \approx t_{\mathrm{LR}}$ as $\hat{a} \to -1$ and $u_{\mathrm{mrg}} < t_{\mathrm{LR}}$ as $\hat{a} \to 1$. See text for details.

IV. KICK AND ANTIKICK

Let us now discuss the recoil velocity computation and the antikick. We define a complex velocity vector $\mathbf{v} \equiv v_x + iv_y$ corresponding to the recoil velocity accumulated by the system up to a certain time t,

$$\mathbf{v} = -\frac{1}{M} \int_{-\infty}^{t} dt' (\mathcal{F}_x^{\mathbf{P}} + i\mathcal{F}_y^{\mathbf{P}}). \tag{7}$$

In practice, the improper integral above is calculated from a finite initial time t_0. Thus the recoil velocity calculation requires us to fix a complex integration constant $\mathbf{v}_0$ that accounts for the velocity that the system has acquired in evolving from $t = -\infty$ to $t = t_0$, i.e.,

$$\mathbf{v} = \mathbf{v}_0 - \frac{1}{M} \int_{t_0}^{t} dt' (\mathcal{F}_x^{\mathbf{P}} + i\mathcal{F}_y^{\mathbf{P}}). \tag{8}$$

If this integration constant is not determined correctly, unphysical oscillations show up in the time evolution of the modulus of the velocity $v(t) \equiv |\mathbf{v}(t)|$, which eventually result in an inaccurate estimate of the final recoil velocity. We determine the vectorial integration constant $\mathbf{v}_0$ by finding the center of the hodograph of the velocity in the complex plane following [3,24]. This procedure is tuned iteratively until the time evolution of $v(t)$ during inspiral grows monotonically without spurious oscillations. The correct determination of the integration constant is especially important when $\hat{a} \to +1$, as it can strongly influence the rather small value of the final recoil velocity.
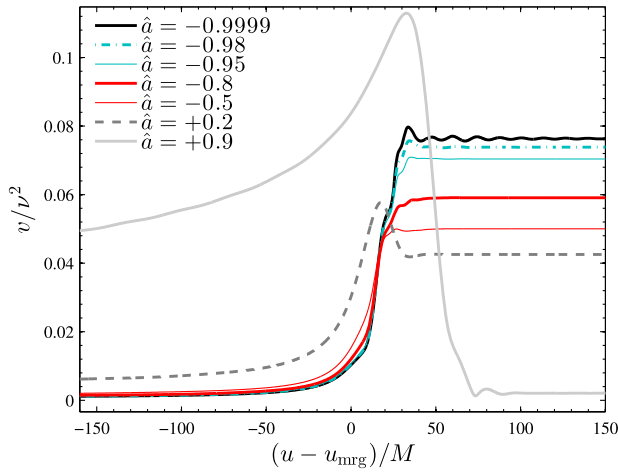

FIG. 4 (color online). Time evolution of the recoil velocity for various values of the black hole spin parameter $\hat{a}$. The large antikick present for positive values of $\hat{a}$ is progressively absorbed until it disappears when $-0.9 \lesssim \hat{a} \lesssim -0.5$. Surprisingly, for nearly extremal negative spins it progressively reappears (see small drop of the solid black line after its global maximum) due to a slight increase of the adiabatic character of the plunge dynamics. We use the location of the peak of $|\Psi_{22}^{(0)}|$ to define the merger time $(u - u_{\mathrm{mrg}})/M = 0$.

Figure 4 shows for some representative configurations $\hat{a} \in \{-0.9999, -0.98, -0.95, -0.8, -0.5, +0.2, +0.9\}$ the time evolution of the recoil velocity. Visually the ascent of the curves is free of oscillations due to the fine-tuned setting of $\mathbf{v}_0$. Close to merger $v(t)$ grows monotonically until it reaches its maximum $v_{\max}$. For large positive spins it then drops down to an asymptotic value $v_{\mathrm{end}} < v_{\max}$. The gap $\Delta v = v_{\max} - v_{\mathrm{end}}$ between the maximal and the final recoil velocity is called the *antikick*. We list in Table I the values of the maximal and final recoil velocities as well as the antikick for the configurations considered in this work.

TABLE I. The column list: the BH spin $\hat{a}$; the magnitude of the maximal and final recoil velocities, $v_{\max}/\nu^2$ and v_{end}/ν^2; the magnitude of the antikick $\Delta v/\nu^2$: for $-0.9 \leq \hat{a} \leq -0.5$ no significant antikick is observed; the quality factor Q associated with the maximum of the amplitude of the linear momentum flux, as an indicator of the adiabaticity of the emission of linear momentum: the larger Q is, the more adiabatic is the emission process, the larger is the antikick; the characteristic time scale $\tau_{\dot{p}_{r_*}}^{\max}$ of $-\dot{p}_{r_*}$ [see Eq. (1)], as a complementary indicator of the adiabaticity of the dynamics; the approximate analytic calculation of the kick velocity, $v_{\mathrm{end}}^{\mathrm{anal}}/\nu^2$ of Eq. (11). Minima of $\Delta v/\nu^2, Q, \tau_{\dot{p}_{r_*}}^{\max}$ are shown in boldface. The (more uncertain) results for nearly extremal positive spins are separated by a horizontal line (see the Appendix).

$\hat{a}$	$v_{\max}/\nu^2$	v_{end}/ν^2	$\Delta v/\nu^2$	Q	$\tau_{\dot{p}_{r_*}}^{\max}$	$v_{\mathrm{end}}^{\mathrm{anal}}/\nu^2$
−0.9999	0.07972	0.07634	3.377e-03	1.0060	3.8436	0.04060
−0.9990	0.07967	0.07637	3.303e-03	1.0065	3.8411	0.04091
−0.9950	0.07884	0.07587	2.972e-03	0.9942	3.8302	0.04052
−0.9900	0.07798	0.07539	2.589e-03	0.9639	3.8171	0.04050
−0.9800	0.07571	0.07383	1.883e-03	0.9518	3.7924	0.04017
−0.9700	0.07452	0.07320	1.326e-03	0.9356	3.7696	0.03996
−0.9500	0.07093	0.07040	5.264e-04	0.9015	3.7292	0.03942
−0.9000	0.06545	0.06539	5.589e-05	0.8663	3.6508	0.03855
−0.8000	0.05910	0.05909	9.332e-06	**0.8378**	3.5570	0.03807
−0.7000	0.05501	0.05501	8.223e-07	0.8402	3.5123	0.03910
−0.6000	0.05183	0.05183	1.915e-08	0.8650	**3.4977**	0.04189
−0.5000	0.05003	0.05003	**2.289e-09**	0.9024	3.5044	0.04765
−0.4400	0.04914	0.04879	3.485e-04	0.9491	3.5167	0.05318
−0.4000	0.04948	0.04882	6.618e-04	1.0038	3.5280	0.05801
−0.3500	0.04889	0.04787	1.024e-03	1.1444	3.5456	0.06704
−0.3000	0.04913	0.04766	1.479e-03	1.9191	3.5667	0.09562
−0.2500	0.04956	0.04730	2.255e-03	1.6508	3.5914	0.10402
−0.2000	0.04981	0.04658	3.224e-03	1.4625	3.6198	0.09148
−0.1000	0.05060	0.04534	5.266e-03	1.4011	3.6878	0.07821
0.0000	0.05319	0.04530	7.892e-03	1.4364	3.7722	0.07029
0.1000	0.05471	0.04377	1.094e-02	1.5086	3.8755	0.06279
0.2000	0.05771	0.04252	1.519e-02	1.6045	4.0019	0.05655
0.3000	0.06105	0.04053	2.052e-02	1.7207	4.1580	0.05116
0.4000	0.06606	0.03822	2.785e-02	1.8678	4.3534	0.04578
0.5000	0.07131	0.03398	3.733e-02	2.0643	4.6049	0.03887
0.6000	0.07796	0.02831	4.965e-02	2.3413	4.9426	0.02766
0.7000	0.08719	0.02056	6.663e-02	2.7528	5.4289	0.01406
0.8000	0.09919	0.01085	8.835e-02	3.5249	6.2242	0.00431
0.9000	0.11293	0.00206	1.109e-01	5.3834	7.8682	0.00031
0.9500	0.11186	0.00065	1.112e-01	7.1404	8.6964	0.00015
0.9700	0.10821	0.00046	1.077e-01	7.9190	8.8428	0.00008
0.9800	0.10524	0.00043	1.048e-01	8.7525	9.0199	0.00021
0.9900	0.10307	0.00044	1.026e-01	9.2251	9.4295	0.00045
0.9950	0.10127	0.00038	1.009e-01	9.3933	9.8429	0.00039
0.9990	0.09968	0.00036	9.933e-02	9.2492	10.4124	0.00019
0.9999	0.09914	0.00035	9.878e-02	9.1388	10.5938	0.00031

The antikick is large for positive spins and essentially absent for $-0.9 \leq \hat{a} \leq -0.5$. Our data highlight a new feature of the antikick for nearly extremal, negative spins: *the antikick "strikes back"* for $-1 < \hat{a} < -0.9$, i.e., Δv increases again, though it reaches smaller values than for positive spins. From the value $\Delta v/\nu^2 \sim 6 \times 10^{-5}$ at $\hat{a} = -0.9$, it rises to 1.3×10^{-3} at $\hat{a} = -0.97$ and reaches $\sim 3.4 \times 10^{-3}$ in the most extremal case considered ($\hat{a} = -0.9999$). This value is comparable to values obtained for $\hat{a} \sim -0.2$. [Note that the uncertainty on $v_{\max}$ yielded by the fine-tuning of $\mathbf{v}_0$ is less than 0.01%.] The behavior of the recoil velocities and the antikick versus $\hat{a}$ is illustrated in Fig. 5. The top panel shows the maximal and final recoil velocities. The SKH fit is included for comparison. The bottom panel shows the antikick. Note that in the range $-0.9 \leq \hat{a} \leq +0.9$ our data are compatible with SKH findings (though slightly different because of different prescriptions for the radiation reaction and different accuracies, see the Appendix).

The reappearance of the antikick, although *a priori* surprising, can be understood qualitatively in relatively simple terms following DG. One of the points of DG was to relate the antikick to the maximum of the modulus of the GW linear momentum flux, $\mathcal{F}_{\mathbf{P}}^{\max} = \max |\mathcal{F}_{\mathbf{P}}|$. At

time t, the accumulated kick velocity is given by the complex integral (7) (with $M = 1$ for simplicity), i.e., $\mathbf{v} = -\int_{-\infty}^{t} |\mathcal{F}_{\mathbf{P}}(t')|e^{i\varphi(t')}dt'$, where $\varphi(t)$ is the phase of the linear momentum flux. Expanding around the time $t_{\max}$ corresponding to $\mathcal{F}_{\mathbf{P}}^{\max}$ one gets

$$\mathbf{v} \simeq -\mathcal{F}_{\mathbf{P}}^{\max} e^{i\varphi_{\max}} \sqrt{\frac{\pi}{2\alpha}} e^{\beta^2/(2\alpha)} \operatorname{erfc}(z), \tag{9}$$

with $z = -\sqrt{\alpha/2}(\bar{t} - \beta/\alpha)$, where $\alpha \equiv 1/\tau_{\max}^2(1 - i\epsilon_{\max})$, $\beta = iQ/\tau_{\max}$ and $\bar{t} = t - t_{\max}$. Here $\tau_{\max}^2 \equiv -\mathcal{F}_{\mathbf{P}}^{\max}/(|\ddot{\mathcal{F}}|_{\mathbf{P}})^{\max}$ is the characteristic time scale associated with the "resonance peak" of $|\mathcal{F}_{\mathbf{P}}|$; $\omega \equiv \dot{\varphi}$, $\epsilon_{\max} \equiv \dot{\omega}_{\max}\tau_{\max}^2$ [where $\dot{\omega}_{\max} \equiv \dot{\omega}(t = t_{\max})$], and the quantity

$$Q \equiv \omega_{\max}\tau_{\max} \tag{10}$$

can be interpreted as the *quality factor* associated with the same peak. According to Eq. (9) the time evolution of the recoil velocity is given by the complementary error function $\operatorname{erfc}(z)$ of a complex argument z whose imaginary part is proportional to the quality factor Q. Hence, the quality factor Q controls the monotonic behavior of $\operatorname{erfc}(z)$: when Q is sufficiently large a local maximum appears.

The values of Q are listed in Table I for all configurations considered. One observes immediately the tight correlations between Q, v_{end}, Δv and $\tau_{\dot{p}_{r_*}}^{\max}$, which supports the interpretation of the antikick results in terms of these analysis tools. The behavior of (Δv, $\tau_{\dot{p}_{r_*}}^{\max}$, Q) versus $\hat{a}$ is qualitatively the same, see Fig. 6: they are maximal as
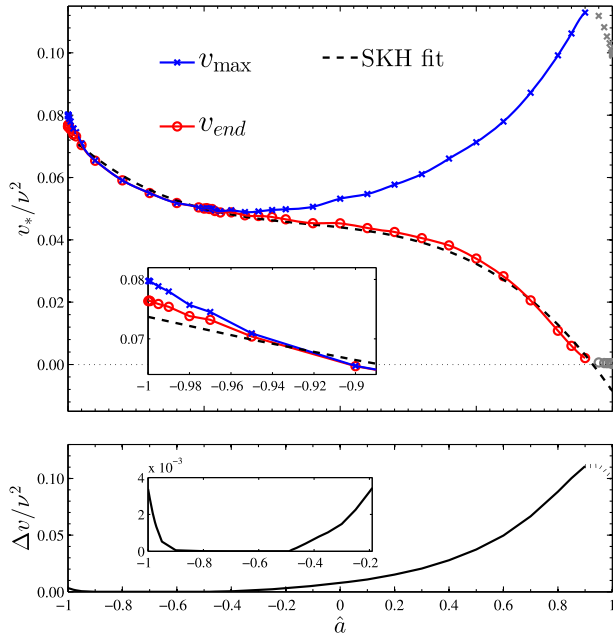

FIG. 5 (color online). Dependence of the maximum (blue, crosses) and the final (red, circles) recoil velocities on the spin $\hat{a}$ for $\nu = 10^{-3}$. The dashed black line refers to the fit of [4]. Although the antikick is suppressed in the interval $-0.9 \leq \hat{a} \leq -0.5$, it strikes back for large negative spins, i.e., for $\hat{a} \lesssim -0.9$ we find again that $v_{\max} > v_{\text{end}}$. The data points for $\hat{a} > 0.9$ are plotted in gray to indicate that they are affected by larger systematic uncertainties due to inaccuracy of the radiation reaction as $\hat{a} \rightarrow +1$ ($v_{\max}$ is expected to grow monotonically; see the Appendix).
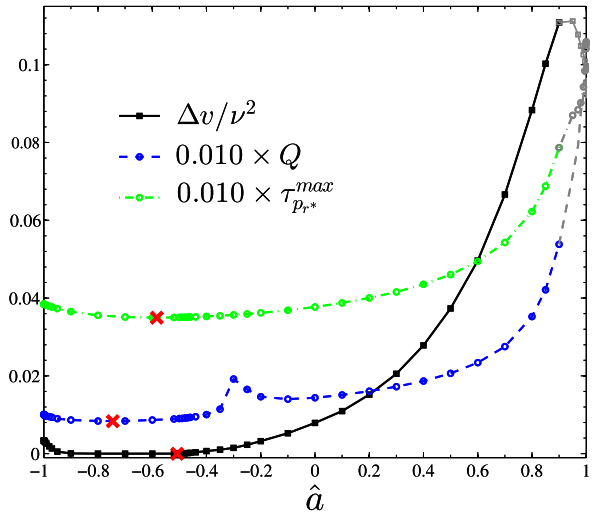

FIG. 6 (color online). Visualizing the data of Table I. The behavior of the (scaled) quantities Q and $\tau_{\dot{p}_{r_*}^{\max}}$ is mirrored by the one of the antikick. The local maximum in Q around $\hat{a} = -0.3$ is due to the particular structure of $|\mathcal{F}_{\mathbf{P}}|$ in that spin range, more precisely a rather shallow top resulting from two peaks of approximately the same height very close or fused together (see Fig. 2 and discussion in text). The big red crosses mark the interpolated minima.

$\hat{a} \to 1$, decrease fast for $0 < \hat{a} < +1$, then decrease further but at a milder rate to generate a rather shallow valley with a global minimum around $\hat{a} = -0.5$ and finally increase again as $\hat{a} \to -1$ (we discuss below the nonmonotonic behavior of Q when $\hat{a} \approx -0.3$). More precisely, the minima are attained at $\hat{a} \sim (-0.5, -0.58, -0.75)$ for, respectively $(\Delta v, \tau_{\dot{p}_{r_*}}^{\max}, Q)$.

Physically the quality factor can be interpreted as a measure of the adiabaticity of the process: small Q indicates fast emission of linear momentum and reduced antikick; large Q indicates slow emission of linear momentum and enhanced antikick. Thus, the computation of Q from the maximum of the linear momentum flux gives us a qualitative method to understand the origin of the antikick and, in particular, to predict its behavior for $\hat{a} \to -1$ (see Fig. 5). Although Q is helpful in understanding the global picture, it might be missing some details. For example, inspecting Fig. 6 and Table I one sees that Q is in one-to-one correspondence with Δv and $\tau_{\dot{p}_{r_*}}^{\max}$ for all values of $\hat{a}$ except in the range $-0.4 < \hat{a} < 0$, where it shows a local maximum instead of growing monotonically as the behavior of Δv (and $\tau_{\dot{p}_{r_*}}^{\max}$) suggest. Actually, inspecting $|\mathcal{F}_{\mathbf{P}}|$ for, say, $\hat{a} = -0.3$ (that shows the largest deviation from the global growing trend) one finds that it has a rather shallow top region, with essentially two maxima of approximately the same height close together instead of one distinguished maximum as for the other cases (see Fig. 2). This corresponds to the onset of the interference pattern in the flux that is well evident for $\hat{a} = -0.9999$, as highlighted in Fig. 2. In this particular case, the approximation that is behind the computation of Q is probably not accurate enough to faithfully represent the structure of the peak of $|\mathcal{F}_{\mathbf{P}}|$.

Finally, following DG, when $t \gg \tau_{\max}$, the error function in Eq. (9) can be evaluated analytically to give the following approximate estimate of the final recoil magnitude

$$v_{\text{end}}^{\text{anal}} \simeq \sqrt{2\pi} \mathcal{F}_{\mathbf{P}}^{\max} \frac{\tau_{\max}}{(1 + \epsilon_{\max}^2)^{1/4}} e^{-Q^2/[2(1+\epsilon_{\max}^2)]}. \quad (11)$$

Looking at Table I the computed $v_{\text{end}}^{\text{anal}}$ is of the same order of magnitude as v_{end} over the whole spin range. Percentual differences usually vary around $\sim 50\%$ but can reach $\sim 10\%$ for values around $\hat{a} \sim 0.6$. It would be interesting to increase the order of the approximation of Eq. (9) and recheck its domain of accuracy depending on $\hat{a}$. Such a formula would simplify the computation of the final recoil from numerical relativity data, especially because one would rely only on local knowledge of the linear momentum flux avoiding the uncertainties related to the integration constant.

V. CONCLUSIONS

In this work we have focused on binary black hole coalescences in the small-mass-ratio limit where the larger black hole is spinning. We have extended the parameter space of the recoil computations of [4] to the nearly extremal negative spin regime $-0.9999 \le \hat{a} < -0.9$. Our main new finding is an unexpected phenomenon that appears in this before unexplored regime: The antikick, i.e., the drop from the maximal to the final recoil velocity, is *not* a monotonic function of the spin and, while suppressed between $-0.9 \le \hat{a} \le -0.5$, it reappears for nearly extremal negative spins.

Quantitatively, this finding is a small but significant effect, in the sense that it returns to values comparable to the moderately spinning configurations with $\hat{a} \sim 0.2$. It can be interpreted and predicted qualitatively by analyzing the plunge dynamics or the GW linear momentum flux around its maximum. The variation of the latter can be measured by the quality factor Q of [7], which is understood to be a measure of the "adiabaticity" of the process of emission of linear momentum through GWs. A significant antikick always results from a slow (quasiadiabatic) plunge and is associated with large values of Q. Small values of Q mirror a rather nonadiabatic plunge and, consistently, small, or absent, antikicks. In this work we have verified for the first time on a large set of data the efficiency of Q as an analysis tool. The fact, that Q is found *a posteriori* to even predict the discovered return of the antikick indicates that it is working in delicate situations.

We have also pointed out how certain features of the linear momentum flux directly mirror the dynamics, so that the reappearance of the antikick allowed us to gain a deeper understanding of the dynamics of retrograde plunges. Incidentally, we have confirmed (and possibly improved), for the first time, the recoil computations of Ref. [4], notably using the analytic effective one body (EOB)-resummed radiation reaction to drive the relative dynamics from quasicircular inspiral to plunge.

Qualitatively, our findings may be robust also in unequal but comparable mass-ratio binaries, in which the ratio between the spin of the two objects is nearly extremal. If the return of the antikick cannot be reproduced in comparable mass-ratio binaries, the question for a limiting mass-ratio arises. In any case, the (gauge-invariant) flux analysis on the basis of the quality factor presented here may guide the extraction of useful information from kick computations in numerical relativity simulations, like those recently performed in [25].

TABLE II. Dependence on ℓ_{max} of v_{end} and v_{max}. For $\hat{a} = -0.9999$, $\ell_{max} > 4$ contributions give less than 1%. For $\hat{a} = +0.9$, the effect is larger and v_{end} slightly increases for higher ℓ_{max}.

		$\hat{a} = -0.9999$		
ℓ_{max}	v_{max}/ν^2	diff (%)	v_{end}/ν^2	diff (%)
2	0.070252	$\cdots$	0.068323	$\cdots$
3	0.077692	10.59	0.074520	9.07
4	0.079033	1.73	0.075589	1.43
5	0.079187	0.19	0.075766	0.23
6	0.079442	0.32	0.076045	0.37
7	0.079613	0.21	0.076228	0.24
8	0.079722	0.14	0.076345	0.15
		$\hat{a} = +0.9$		
ℓ_{max}	v_{max}/ν^2	diff (%)	v_{end}/ν^2	diff (%)
2	0.003687	$\cdots$	0.000932	$\cdots$
3	0.045957	1146.49	0.001190	27.80
4	0.074009	61.04	0.001350	13.43
5	0.091701	23.90	0.001535	13.64
6	0.102239	11.49	0.001741	13.44
7	0.108800	6.42	0.001917	10.10
8	0.112927	3.79	0.002056	7.27

APPENDIX: ACCURACY

We give here some estimates about the accuracy of our computation and discuss the limitations of our approach for configurations with $\hat{a} \to +1$.

Table II shows the effect of ℓ_{max} on the velocity computation. The results for $\hat{a} = -0.9999$ vary $\lesssim 1\%$ by including multipoles with $\ell_{max} > 4$. The inclusion of high multipoles is more relevant for large positive spins. For $\hat{a} = +0.9$ we observe an $\sim 7\%$ variation by increasing $\ell_{max} = 7$ to $\ell_{max} = 8$. Including only up to $\ell_{max} = 6$ multipoles underestimates v_{end} by at least 10%. This is consistent with the corresponding variations we see in the

fluxes, Fig. 2. Note that v_{end} increases by including more multipoles.

Another source of uncertainty is the finite value of the mass ratio ν employed in the simulations [3]. Table III shows a comparison between results obtained with $\nu = 10^{-3}$ and $\nu = 10^{-4}$. The uncertainties for $\hat{a} < 0.5$ are at the 1% level. For larger spins they grow and reach about 7% for $\hat{a} = 0.9$. We expect even larger uncertainties for $\hat{a} \geq 0.95$ since these simulations are strongly biased by the inaccurate radiation reaction (see below).

Our kick calculation in Table I and Fig. 5 can be compared with the fit proposed in SKH. The latter was calculated (i) including multipoles up to $m_{max} = 6$, (ii) using a different technique to determine the integration constant, (iii) using $\nu = 10^{-4}$ simulations of about 25 orbits, and (iv) a series of circular geodesics for the inspiral. The fit of SKH refers to the interval $|\hat{a}| < 0.9$ and is therein consistent with our data, in some cases within 1%. However, it does not capture the fine structures for nearly extremal values of the spin. Observe, for example, that it underestimates v_{end} for $\hat{a} \to -1$ (Fig. 5).

Let us finally discuss the data for nearly extremal positive spins $+0.9 < \hat{a} \leq +0.9999$. These data are displayed in Fig. 5 in gray color since they are uncertain. The numbers behind the plot are therefore listed separately in Table I. Inspecting the table and Fig. 5 one sees that (i) v_{end} first decreases and then remains approximately constant (and very small) for $\hat{a} \geq 0.995$, (ii) v_{max} *decreases* monotonically, (iii) Q oscillates around 9.2 for $0.99 \leq \hat{a} \leq 0.9999$, and (iv) $\tau_{\dot{p}_{r_*}}^{max}$ increases monotonically. At first sight these numbers look contradictory. The increase of $\tau_{\dot{p}_{r_*}}^{max}$ with $\hat{a}$ is indicating that the dynamics (and thus the emission of linear momentum) is increasingly adiabatic as $\hat{a} \to +1$. Consistently, v_{end} decreases, but the increased adiabaticity of the dynamics is not mirrored in Q or in v_{max}, which decreases instead.

A careful inspection of the dynamics brought us to conclude that these results are *qualitatively inaccurate* for v_{max} (and thus Q) and *quantitatively inaccurate* for v_{end}. The main reason is the systematic inaccuracy of the radiation reaction for large positive spins $\hat{a} \gtrsim 0.9$, as shown in [6]. Practically speaking, the low accuracy of the

TABLE III. Effect of the mass ratio ν. The table compares for a few values of $\hat{a}$ the recoil velocities as obtained from trajectories with $\nu = 10^{-3}$ and $\nu = 10^{-4}$. The percentage difference is about 1% for $\hat{a} < 0.9$ and reaches $\sim 7\%$ for $\hat{a} = 0.9$. We use the notation $v^{(\log_{10}\nu)}$.

$\hat{a}$	$v_{max}^{(-3)}/\nu^2$	$v_{max}^{(-4)}/\nu^2$	diff (%)	$v_{end}^{(-3)}/\nu^2$	$v_{end}^{(-4)}/\nu^2$	diff (%)
-0.9000	0.06545	0.06598	0.81	0.06539	0.06592	0.81
-0.7000	0.05501	0.05504	0.06	0.05501	0.05504	0.06
-0.5000	0.05003	0.04964	0.76	0.05003	0.04964	0.76
0.0000	0.05319	0.05313	0.11	0.04530	0.04508	0.48
0.5000	0.07131	0.07119	0.17	0.03398	0.03383	0.44
0.7000	0.08719	0.08877	1.81	0.02056	0.02073	0.83
0.9000	0.11293	0.12093	7.09	0.00206	0.00199	3.24

radiation reaction (and in particular the absence of horizon fluxes that could contrast the loss of angular momentum to infinity via superradiance [16,26]) makes the system lose too much angular momentum. For $\hat{a} > +0.97$ this effect is so strong that the angular momentum p_ϕ becomes *negative* ($p_\phi \sim -0.1$) around merger. For example, for $a + 0.9999$ (see Fig. 7) this change of sign occurs at $t/M = 5038$, that is quite close to the peak of the flux of linear momentum in a domain where the waveforms are still influenced by the dynamics (the LSO is crossed at $t/M = 5056.6$ and the light ring at $t/M = 5220$). This unphysical effect (p_ϕ is defined to be positive) mirrors an excessive acceleration of the dynamics during the plunge and heuristically explains the drop of $v_{\max}$ for $\hat{a} > 0.9$. By contrast, we found that the calculation of $\tau_{\dot{p}_{r_*}}^{\max}$ relies on a part of the dynamics before the change of sign of p_ϕ ($-\dot{p}_{r_*}$ peaks at $t/M = 5028$) and therefore is more robust, as confirmed by the monotonic behavior of $\tau_{\dot{p}_{r_*}}^{\max}$ over $\hat{a}$. A way of treating larger spin values is to adopt the self-consistent radiation reaction method introduced in [6]. Doing this is computationally very demanding and will be discussed in a follow-up study. At present, we could check our understanding only against self-consistent $\hat{a} = +0.9$ data [6]. Consistent with our expectation that the correct radiation reaction should yield a more adiabatic plunge, we found a slightly smaller $v_{\rm end}^{\rm sc}/\nu^2 = 0.00189$ (instead of 0.00206) and a
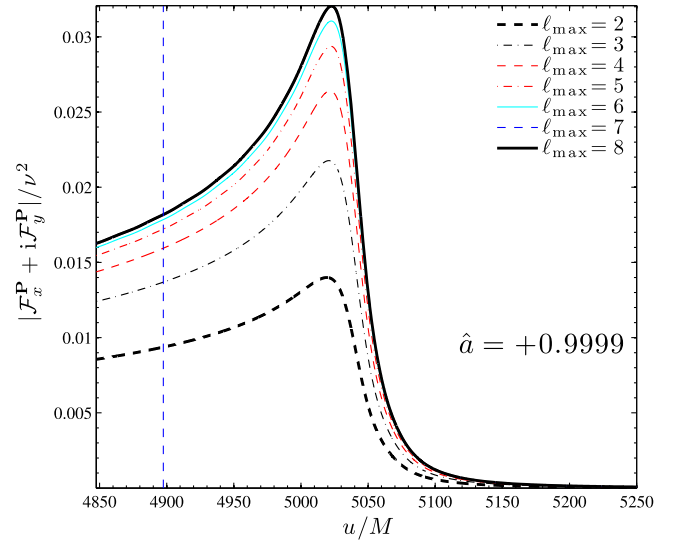

FIG. 7 (color online). Flux of linear momentum for $\hat{a} = +0.9999$. The vertical line indicates the peak of $|\Psi_{22}|$.

slightly larger $v_{\max}^{\rm sc}/\nu^2 = 0.11908$ (instead of 0.11293). This preliminary result suggests that $v_{\max}$ will increase further and $v_{\rm end}$ will become smaller as $\hat{a} \to +1$. New, challenging investigations will be needed to answer the question, whether $v_{\rm end} = 0$ for $\hat{a} = +1$ as our results seem to indicate.

[1] J. D. Schnittman, A. Buonanno, J. R. van Meter, J. G. Baker, W. D. Boggs, J. Centrella, B. J. Kelly, and S. T. McWilliams *et al.*, Phys. Rev. D **77**, 044031 (2008).

[2] A. Nagar, Phys. Rev. D **88**, 121501 (2013).

[3] S. Bernuzzi and A. Nagar, Phys. Rev. D **81**, 084056 (2010).

[4] P. A. Sundararajan, G. Khanna, and S. A. Hughes, Phys. Rev. D **81**, 104009 (2010).

[5] J. G. Baker, J. Centrella, D.-I. Choi, M. Koppitz, J. R. van Meter, and M. C. Miller, Astrophys. J. **653**, L93 (2006).

[6] E. Harms, S. Bernuzzi, A. Nagar, and A. Zenginoglu, Classical Quantum Gravity **31**, 245004 (2014).

[7] T. Damour and A. Gopakumar, Phys. Rev. D **73**, 124006 (2006).

[8] R. H. Price, G. Khanna, and S. A. Hughes, Phys. Rev. D **83**, 124002 (2011).

[9] R. H. Price, G. Khanna, and S. A. Hughes, Phys. Rev. D **88**, 104004 (2013).

[10] L. Rezzolla, R. P. Macedo, and J. L. Jaramillo, Phys. Rev. Lett. **104**, 221101 (2010).

[11] T. Damour and A. Nagar, Phys. Rev. D **90**, 044018 (2014).

[12] A. Nagar, T. Damour, and A. Tartaglia, Classical Quantum Gravity **24**, S109 (2007).

[13] T. Damour, B. R. Iyer, and A. Nagar, Phys. Rev. D **79**, 064004 (2009).

[14] Y. Pan, A. Buonanno, R. Fujita, E. Racine, and H. Tagoshi, Phys. Rev. D **83**, 064003 (2011).

[15] A. Nagar and S. Akcay, Phys. Rev. D **85**, 044025 (2012).

[16] A. Taracchini, A. Buonanno, S. A. Hughes, and G. Khanna, Phys. Rev. D **88**, 044001 (2013).

[17] A. Taracchini, A. Buonanno, G. Khanna, and S. A. Hughes, Phys. Rev. D **90**, 084025 (2014).

[18] E. Harms, S. Bernuzzi, and B. Brügmann, Classical Quantum Gravity **30**, 115013 (2013).

[19] A. G. Shah, Phys. Rev. D **90**, 044025 (2014).

[20] A. Buonanno and T. Damour, Phys. Rev. D **62**, 064015 (2000).

[21] D. Bini and T. Damour, Phys. Rev. D **86**, 124012 (2012).

[22] S. Hod, Phys. Rev. D **61**, 064018 (2000).

[23] W. Krivan, P. Laguna, P. Papadopoulos, and N. Andersson, Phys. Rev. D **56**, 3395 (1997).

[24] D. Pollney, C. Reisswig, L. Rezzolla, B. Szilagyi, M. Ansorg *et al.*, Phys. Rev. D **76**, 124002 (2007).

[25] J. Healy, C. O. Lousto, and Y. Zlochower, Phys. Rev. D **90**, 104004 (2014).

[26] S. Bernuzzi, A. Nagar, and A. Zenginoglu, Phys. Rev. D **86**, 104038 (2012).